Carbon 189 (2022) 422–429

Contents lists available at ScienceDirect

Carbon

journal homepage: www.elsevier.com/locate/carbon

Dynamics and structural transformations of carbon onion-like structures under high-velocity impacts

M.L. Pereira Júnior [a], W.F. da Cunha [a], R.T. de Sousa Junior [b], G.D. Amvame Nze [b], D.S. Galvão [c, d], L.A. Ribeiro Júnior [a, *]

[a] Institute of Physics, University of Brasília, Brasília, 70919-970, Brazil
[b] Department of Electrical Engineering, University of Brasília, 70919-970, Brazil
[c] Applied Physics Department, University of Campinas, Campinas, São Paulo, Brazil
[d] Center for Computing in Engineering and Sciences, University of Campinas, Campinas, São Paulo, Brazil

ARTICLE INFO

Article history:
Received 14 September 2021
Received in revised form
30 November 2021
Accepted 17 December 2021
Available online 27 December 2021

Keywords:
Carbon nano-onion
High-velocity impact
Diamondoid
Fullerene

ABSTRACT

Carbon nano-onions (CNO) are multilayered fullerenes. They exhibit good electrical conductivity and large surface area, being of interest for several optoelectronic applications. However, it is still an open question what synthesis routes can be used to convert them into diamonds. Here, we used fully atomistic reactive (ReaxFF) molecular dynamics simulations to study the dynamics and structural transformations of CNO structures under high-velocity impacts against a fixed and rigid substrate. The aim of this study is to propose a new synthesis route, based on the mechanical impact of CNO, that can be exploited in the conversion of onions to diamonds. Our results indicated three regimes formed after the CNO impact: slightly deformed CNO (quasi-elastic collision, below 2.0 km/s), collapsed CNO (inelastic collisions, between 3.0 and 5.0 km/s) forming a diamondoid-like core, and fragmented CNO yielding linear atomic carbon chains (above 5.0 km/s). We also discussed the dynamical reconfiguration of carbon-carbon bonds during the collision process. The impact of CNO yielded sp^3-like bond types for all the used initial velocities. At intermediate velocities (between 3.0 and 5.0 km/s), the inelastic collision forms diamondoid-like cores by converting a substantial quantity of sp^2-like bonds into sp^3-like ones.

1. Introduction

Different types of carbon-based materials have been the subject of great interest from the scientific community due to their unique properties and potential applications [1,2]. As a result, a substantially increased understanding of systems as diverse as conjugated polymers [3], carbon nanotubes [4], graphene nanoribbons [5], and fullerenes [6] has been achieved. Studies on their structural and electronic properties from both experimental [7–11] and theoretical [12–15] points of view stand out. These features are considered crucial for improving electrochemical energy storage [16,17] and conversion [18,19] processes in the electronics field.

The fullerenes discovery in the early 80s [4] triggered the synthesis of a novel carbon allotrope based on C_{60} in the 90s. Ugarte reported multilayered fullerenes by working with curved graphitic networks, today known as Carbon Nano-Onions (CNO) [20]. These systems exhibit a unique combination of structural and electronic properties [21]. CNO are quasi-spherical nanostructures composed of multiple enclosed concentric fullerene shells (in a close analogy to the layers of an actual onion, see Fig. 1) [21]. Diamond-like core structures have also been observed [22]. These systems present high electrical conductivity levels and a large surface area when contrasted with other nanomaterials [21]. Their relatively easy synthesis provides a level of controllability that allows efficient functionalization procedures [23–25]. Such properties have made CNO good candidates for a wide range of applications, such as biological imaging and sensing [26,27], environmental remediation [28,29], electronics (as batteries, capacitors, fuel cells, and terahertz-shielding devices) [23,30], catalysts [31], tribology [32], optical limiting [33], and molecular junctions in STM [34].

The transformation process of nano-diamonds annealed up to 2270 K into CNO was studied using X-ray diffraction and molecular dynamics simulations [35]. It was obtained that the conversion of the outer diamond-like part into the icosahedral or quasi-icosahedral fullerenes occurred between 1670 K and 1970 K. This

* Corresponding author.
E-mail address: ribeirojr@unb.br (L.A. Ribeiro Júnior).

https://doi.org/10.1016/j.carbon.2021.12.064
0008-6223/

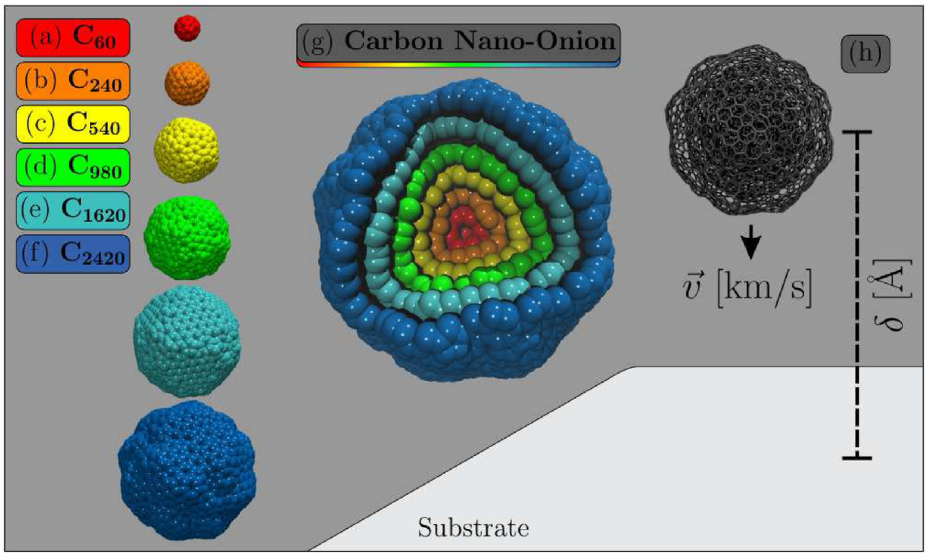

Fig. 1. Schematic representation of the structural models of the carbon nano-onions used here. (a–f) illustrate the single structures (shells) that compose the full CNO, in which the number of carbon atoms varies from 60 up to 2420. The biggest multi-shell CNO has 5860 atoms. (g) depicts the composition of the CNO. (h) shows our initial simulation setup for the CNO/substrate system in which $\delta = 50$ Å. This CNO structure was created based on reference [49]. (A colour version of this figure can be viewed online.)

process was triggered by the graphitization process started from the outer part of nano-diamonds. At higher temperatures, the initial diamond atomic arrangement is converted completely into the sequence of the fullerene shells [35]. In another experimental study, small CNO was prepared by annealing nano-diamonds in an argon atmosphere [36]. The structure and morphology of CNO were determined by X-ray diffraction, and high-resolution transmission electron microscopy (HRTEM), and the average grain size of the CNO was about 8 nm [36]. These studies demonstrate that there is a pathway for converting diamonds into fullerenes. Nonetheless, mechanisms for performing the opposite pathway of synthesis (i.e, for converting onions into nanodiamonds) remain not fully explored.

In experimental studies, Banhart and Ajayan found that intense irradiation of onion shells by an electron beam resulted in the formation of diamond structure in the onion core [22,37,38]. Through molecular dynamics simulations, the stability of C_{60} and C_{60}, C_{70}, and C_{84} during collisions with a diamond surface were studied by Mowrey [39] Beck [40] and their coworkers, respectively. The results revealed that for low values of collision energy, only nonreactive collisions occur. At higher energies, nonreactive scattering or other two final products are yielded: (1) exchange of one or more atoms between the molecule and the surface or (2) chemisorption of the fullerene molecules. Within the time scale and the range of collision energies adopted, no dissociation of the rebounding molecules was observed. Although this study used isolated fullerenes, the results have paved the way to study the collision of CNO against a substrate. In another theoretical study, Ponomareva and Chernozatonskii proposed a mechanism for converting an onion core into a diamond-like structure [41]. They used molecular dynamics simulations to combine two transformation processes: annealing and atom removal. Within this simulation protocol, they concluded that the transformation of CNO core into diamond is a direct transition from graphite to diamond. In these works, one can note that the transformation of CNO into diamond is of great technical interest [42,43]. A clear feature is that the conventional methods of producing diamonds from graphite discussed in the literature so far require very high pressure, high temperature, and the presence of catalysts. Due to these reasons, there is still a search for a way of converting CNO into diamonds that can neglect these extreme conditions.

It is well-known that materials can have their properties considerably altered when subjected to extreme conditions [44]. The changes are highly dependent on their structural nature and the conditions applied to them. The high-velocity impact of nanostructures can give rise to a myriad of structural deformations, as it was demonstrated for the cases of nanotubes [45,46] and nanoscrolls [47,48]. This technique has even been considered a viable mechanism for synthesizing different materials with a whole different set of properties [44,47]. As mentioned above, It is still an open question what synthesis routes can be used to convert them into diamonds. In this sense, here, we are proposing a new route to convert CNO into diamonds that is based on a physical process, i.e., the mechanical impact of CNO against a substrate.

In this work, we carried out fully atomistic reactive (ReaxFF) molecular dynamics simulations to investigate the high-velocity impact of CNO into a rigid substrate. The aim of this study is to propose a new synthesis route, based on the mechanical impact of CNO against a substrate, that can be exploited in the conversion of onions to diamonds under standard temperature and pressure conditions. To address this collision processes, we study in detail the structural, energetic, and stress aspects of these CNO/substrate impacts.

2. Methodology

We carried out fully atomistic reactive (ReaxFF) Molecular Dynamics simulations [50,51] to investigate the impact of multi-shell CNO and their isolated shells (C_N fullerenes, where N stands for the number of atoms). Such simulations were conducted using the ReaxFF potential as implemented in the Large-scale Atomic/Molecular Massively Parallel Simulator (LAMMPS) [52]. The nanostructures obtained from Ref. [49] were edited to isolate the shells and smaller CNO using the Visual Molecular Dynamics (VMD) software [53].

The typical CNO structure considered in this work is composed of an innermost shell of aC_{60} enclosed by a varying number — from two up to seven — of concentric fullerenes. In Fig. 1 we present a

schematic representation of a CNO with six shells, in which the number of carbon atoms varies from 60 up to 2420 atoms. The biggest multi-shell CNO has 5860 atoms. The CNO are formed by the composition of the different shells. The number of carbon atoms is included in the notation describing each CNO. As mentioned before, CNO_N corresponds to a CNO composed of a particular number of shells. *N* denotes the sum of the carbon atoms in these shells, from the smallest to the biggest fullerenes following the sequence shown in Fig. 1 (e.g., CNO_{300} is a CNO composed by two shells: C_{60} and C_{240}). Our goal is to investigate the dynamics of the systems collision at different velocities with a fixed and rigid substrate. The CNO center of mass is initially placed 50 Å from the substrate.

The rigid substrate is considered using a fixed (time-independent) 12-6 Lennard-Jones potential. Such potential was parameterized using 10 Å cutoff distance, 0.07 kcal/mol of interaction strength, and 3.55 Å distance between the particles for their interaction. We would like to stress that some specific aspects of the system could depend on the substrate. However, we opted for a van der Waals wall to allow a more general analysis and to contrast our results with other works in the literature where this approach was also used [45,46].

We adopted a non-periodic unit cell with such repulsive potential between the nanostructures and the model substrate. We made use of a microcanonical (NVT) ensemble — to thermally equilibrate all structures at 300 K before the collision — and a microcanonical (NVE) ensemble [54] for simulating the impact, considering the fixed time step of 0.1 fs. The simulations were carried out during 10–50 ps, depending on the shooting velocity.

3. Results

The collision process of isolated shells and multi-shell CNO on a rigid substrate were investigated here. Each shell is a fullerene composed of between 60 and 2420 atoms. The multi-shell CNO considered in this work are composed of two up to seven shells, thus having from 300 up to 5860 carbon atoms, totaling 77 cases investigated, subjected to shooting velocities varying from 1.0 up to 7.0 km/s.

The investigated systems were the following: As isolated shells, we considered C_{60}, C_{240}, C_{540}, C_{980}, C_{1620} and C_{2420}. Also, the following multi-shell CNO were studied: CNO_{300} (two shells: C_{60} + C_{240}), CNO_{840} (three shells: CNO_{300} + C_{540}), CNO_{1820} (four shells: CNO_{840} + C_{940}), CNO_{3340} (five shells: CNO_{1820} + C_{1620}), CNO_{5860} (six shells: CNO_{3340} + C_{2420}).

Fig. 2 shows the representative MD snapshots (taken at 4.0 ps of simulation) for the impact of the fullerenes raging from C_{60} up to CNO_{3440}, shooting velocity of 5.0 km/s. The collisions occurred before this time for all cases. The figure is divided into two panels. The upper panel shows a general view of the structure resulting from the collision. The lower one presents a cross-section view of the shells and multi-shell CNO to indicate the internal structural changes resulting from the impact. As a general trend, it is possible to observe that isolated shells possess very distinct deformation pattern dynamics. This trend is not true for the multi-shell CNO since the larger systems are less deformable than smaller ones.

We now discuss the case of the biggest multi-shell CNO considered in this work: CNO_{5860}. In Fig. 3, we compare the collisions results for 2.0, 5.0, and 7.0 km/s shooting velocity values. The

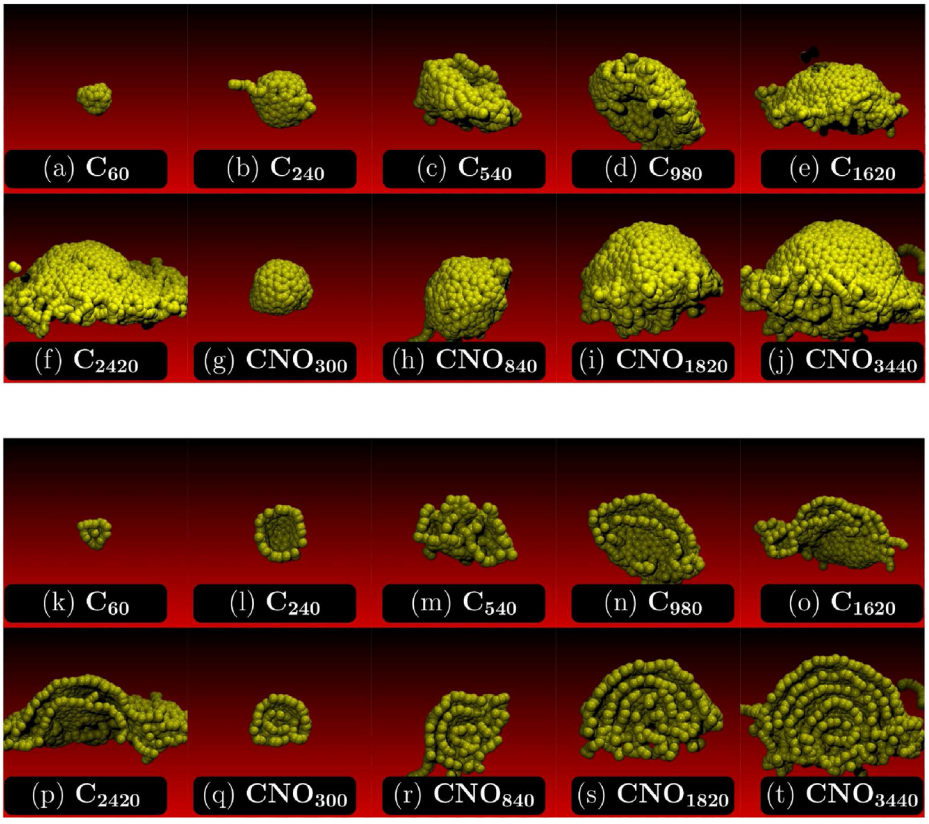

Fig. 2. Representative MD snapshots for (a–f) the isolated shells and (g–j) for the CNO after their impacts. Here, CNO_N corresponds to a CNO composed of a particular number of shells. *N* denotes the sum of the carbon atoms in these shells, from the smallest to the largest fullerenes following the sequence shown in Fig. 1 (e.g., CNO_{300} is a CNO composed by two shells: C_{60} and C_{240}). In these cases, the shooting velocity is 5.0 km/s (a–j) and (k–t) show front views and the corresponding cross-section views of the isolated shells, respectively. (A colour version of this figure can be viewed online.)

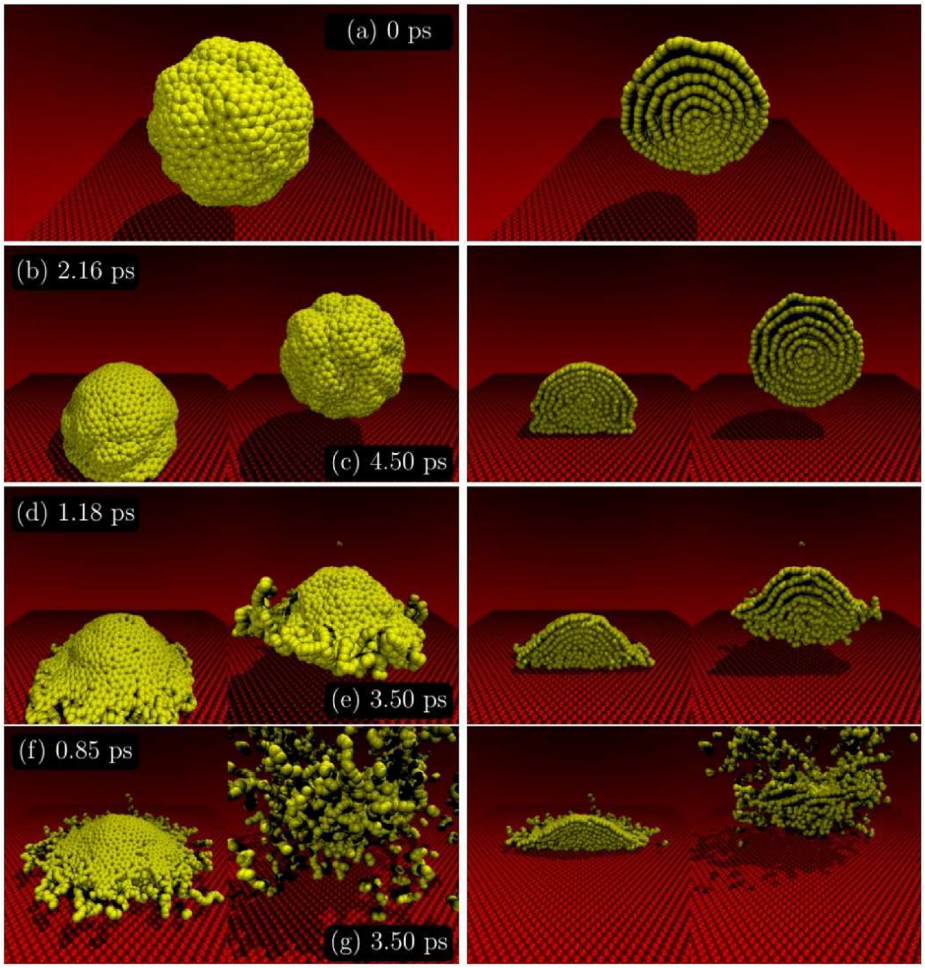

Fig. 3. Representative MD snapshots for the multi-shell CNO (CNO_{5860}) impact at different shooting velocities: 2.0 km/s (top panels), 5.0 km/s (middle panels), 7.0 km/s and (bottom panels). The left and right panels illustrate the front views and their corresponding cross-section views, respectively. The Supplementary Material shows the videos of the simulations for all the cases illustrated in this figure. (A colour version of this figure can be viewed online.)

general and cross-section views are presented in the left and right panels, respectively. The chosen velocities are representative of three observed regimes. Supplementary Material shows the videos of the simulations for all the cases illustrated in this figure. At low velocities, up to 2 km/s, we observed quasi-elastic collisions. It is worthwhile mentioning that the quasi-elastic term designates a limiting case for the inelastic collision, in which a slightly deformed CNO was obtained after the collision process. In this case, the CNO deformation can not be completely reversed. This trend is clear comparing the original structure (Fig. 3(a)) to the resulting ones (Fig. 3(b) and (c)). At intermediate velocities, between 3.0 and 5.0 km/s (see Fig. 3(d) and (e)), inelastic collision occur, as evidenced by the substantial structural deformations. Finally, further increasing the velocities resulted in collapsed/fragmented structures, as can be seen in Fig. 3(f) and (g). These regimes are similar to the ones reported for the cases of nanotubes [45,46] and nanoscrolls [47,48].

To gain further insights into the CNO collision mechanisms, we analyzed the stress per atom pattern (the von Mises Stress) during the impact (Fig. 4), for the cases discussed in Fig. 3 (the CNO_{5860} collision using 2.0 (Fig. 4(b) and (c)), 5.0 (Fig. 4(d) and (e)), and 7.0 km/s (Fig. 4(f) and (g)) as shooting velocities). In the color scheme adopted for this figure, white and red colors denote regions with null and maximum stress values per atom, respectively. The Von Mises stress is calculated accordingly to the procedure described in reference [55]. In Fig. 4(a), one can observe that the optimized structures of the model CNO used here are intrinsically stressed, as expected. At low velocities, up to 2 km/s (Fig. 4(b) and (c)), the stress per atom pattern does not change substantially after the collision. In this way, the quasi-elastic collisions can preserve regions with null stress (white regions). For the inelastic collisions, the CNO structure accumulates a significant amount of stress. Due to its topology, the stress accumulation is almost equally distributed over its surface after the collision, as illustrated in Fig. 4(d–g). This trend for the distribution of the accumulated stress revealed that our model CNO does not present a most probable fracture point (or region). In carbon nanotubes, for instance, the stress accumulation during the impact can occur at the edge or in the center of the nanostructure yielding bilayer graphene or a graphene membrane, respectively [46].

In Fig. 5 we present the time evolution for the total number of different carbon-carbon bond types present in the CNO_{5860} structure. Fig. 5(a), (b), and (c) shows the total number of bonds (sp^1-like, sp^2-like, and sp^3-like) for the impact of the nanostructure with initial velocities of 2.0, 5.0, and 7.0 km/s, respectively. In Fig. 5(a), one can observe that the initial CNO_{5860} configuration only presents sp^2-like-like carbon-carbon bonds, as expected. At low velocities (up to 2 km/s), almost 1000 bonds were converted from sp^2-like-like to sp^3-like ones after the quasi-elastic collision, as shown in Fig. 5(a). The coexistence of sp^2-like and sp^3-like bond types

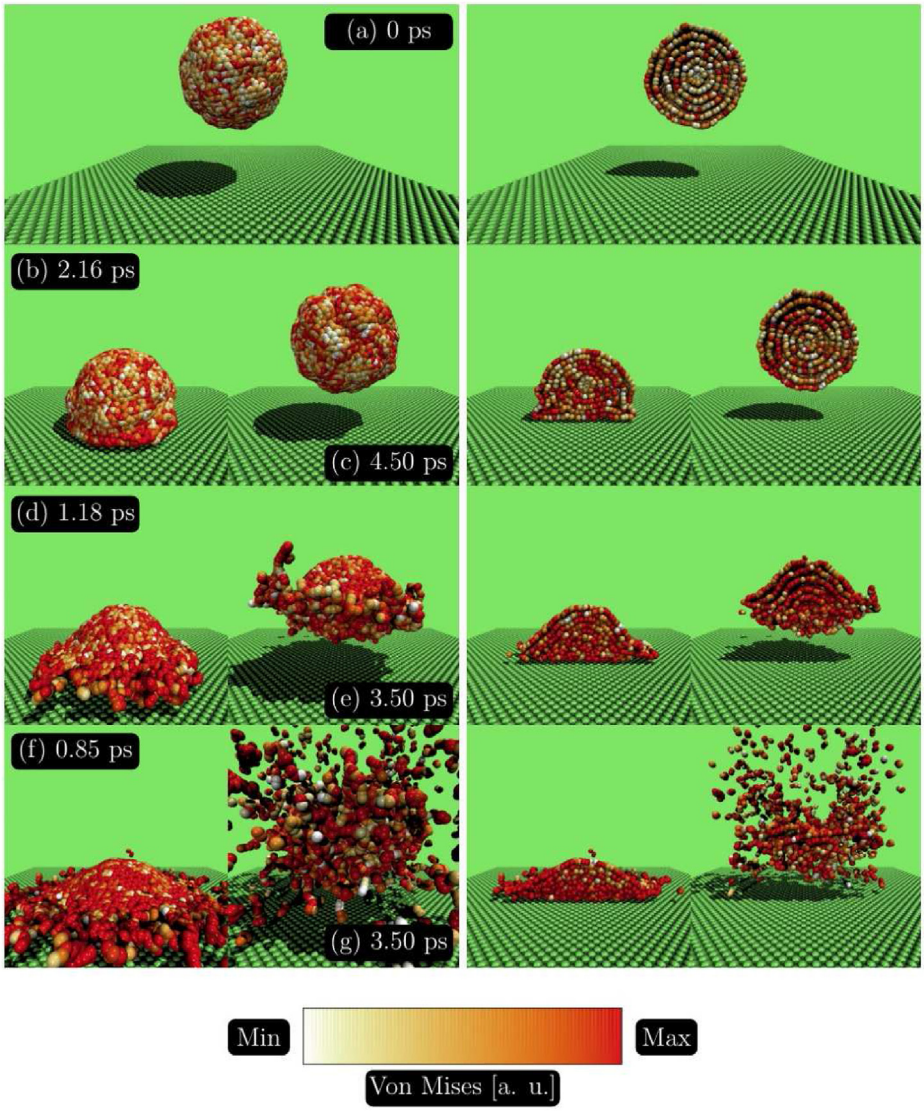

Fig. 4. von Mises stress distribution as a function of the simulation time for the multi-shell CNO (CNO_{5860}) impact at different shooting velocities: 2.0 km/s (top panels), 5.0 km/s (middle panels), 7.0 km/s and (bottom panels). The left and right panels illustrate the front views and their corresponding cross-section views, respectively. (A colour version of this figure can be viewed online.)

remained until the end of the simulation, but with a predominance of sp^2-like bonds, indicating only small CNO_{5860} structural deformations for low velocities. In this figure, a small number of sp^1-like bonds were also observed due to the formation of linear atomic carbon chains (LACS) (see Fig. 3(e)). Importantly, LACS present the chemical structure with alternating short (double or triple bonds) and long C—C bonds (single bonds). They are composed of sp^1 hybridized carbon atoms.

For the high velocities regime (Fig. 5(c)), the total number of sp^1-like, sp^2-like, and sp^3-like bonds tend to be similar, but with a substantial decrease in the quantity of sp^1-like and sp^2-like bonds with relation to the two previous cases. The total number of sp^1-like bonds increased due to a higher degree of fragmentation of the CNO_{5860} and subsequent LACS formation (see Fig. 3(g)).

One striking result was the observation of the formation of a diamondoid-like core depending on the impact velocity. In Fig. 6(a,c), we illustrate representative MD snapshots showing these cores for the shooting velocities of 5 and 7 km/s. For the sake of clarity, the yellow bonds denote the diamondoid-like core, and their zoomed view is presented in the right panels, Fig. 6(b,d). Interestingly, all the CNO shells contributed to the diamondoid-like core formation. This behavior is a relevant result in the sense that it suggests a new synthesis route, based on mechanical impact, that can also be exploited in the conversion of onions to diamonds. Video CNO_DIAMOND.mp4 in Supplementary Material, illustrates that, at least, a small fragment of each CNO shell contributes to forming the diamondoid core. Although not always present in the experimentally realized CNO, some CNO with a diamondoid-like core has been experimentally observed [22,37,38].

Finally, in Fig. 7(a–e), we present the kinetic and potential energy profiles as a function of the simulation time for the multi-shell CNO structures using 5 km/s of shooting velocity as a representative case. Fig. 7(f) shows the time required for converting kinetic into potential energy for the C_N (yellow line) and CNO_N (black line) cases. The total potential energy was shifted to zero by subtracting the CNO ground state energy. In this sense, we are discussing the potential energy gain coming from the conversion of kinetic energy. Fig. 7(f) presents the time required for the multi-shell CNO

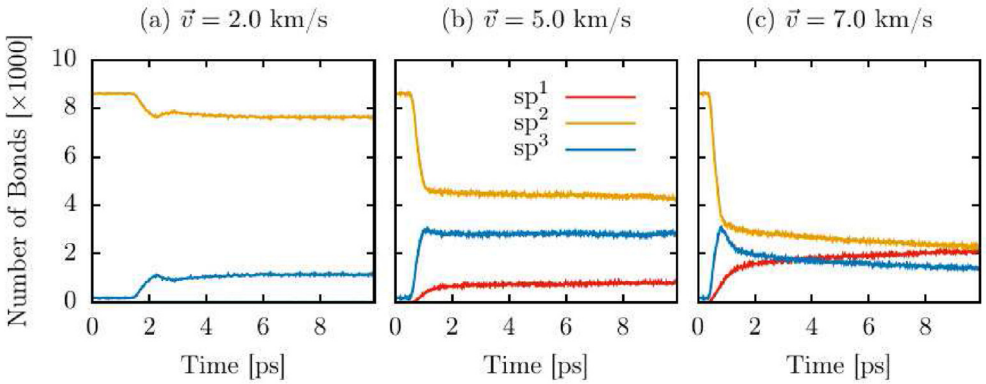

Fig. 5. Time evolution for the total number of different carbon-carbon bond types of the CNO_{5860} system during the collision process. (A colour version of this figure can be viewed online.)

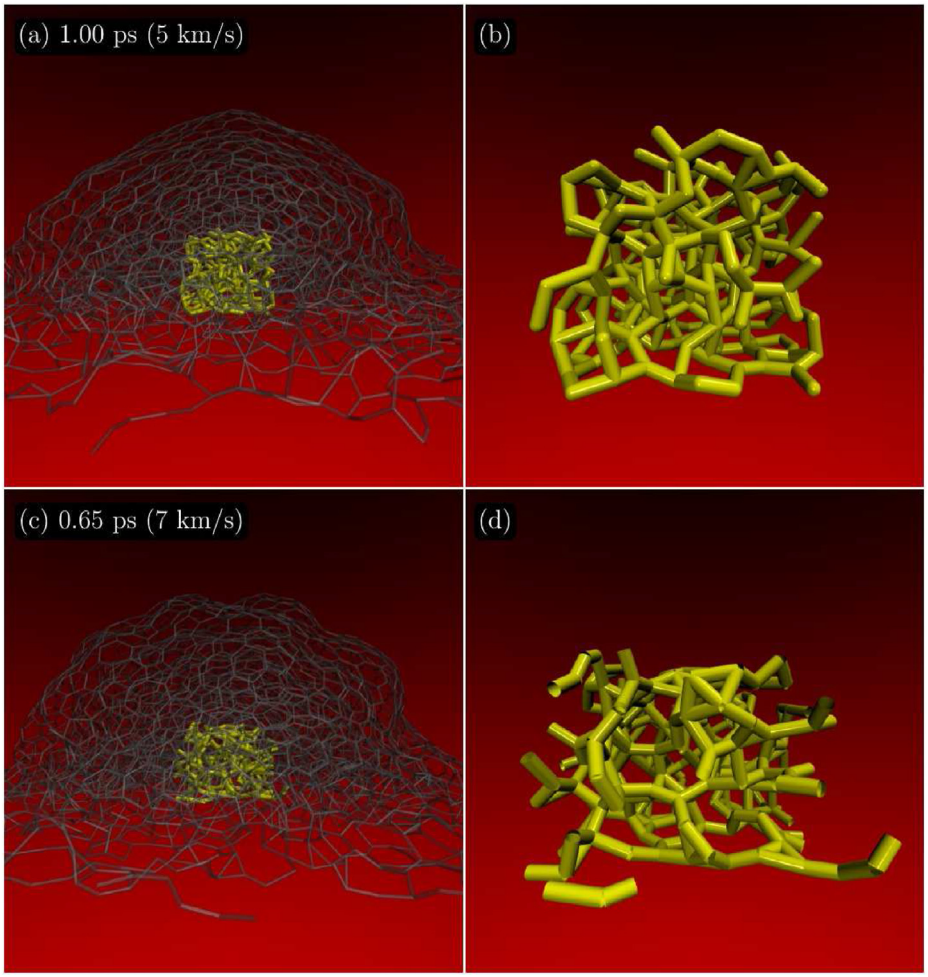

Fig. 6. Representative MD snapshots illustrating the formation of diamondoids after the CNO_{5860} collision at (a–b) 5 km/s and (c–d) 7 km/s. For clarity, the yellow bonds illustrate the diamondoid-like cores, and their zoomed view is presented in the right panels (b–d). (A colour version of this figure can be viewed online.)

investigated here to convert their kinetic to potential energy (i.e., the conversion time during deformation). The CNO degree of deformability tends to increase when their size (i.e., the number of shells) increases. The CNO_{300} and CNO_{840} systems present an abrupt conversion between kinetic and potential energy (see Fig. 7(a) and (b), respectively), that is related to the small size of the systems. For the CNO_{1820}, CNO_{3440}, and CNO_{5860} cases (see Fig. 7(c), (d), and (e), respectively), the conversion between these energies occurs smoothly, despite their smaller deformability when contrasted to the CNO_{300} and CNO_{840} cases. The big CNO (Fig. 7(a) and (b)) interact with the substrate earlier than the small ones (Fig. 7(c–e)). For the size of the model fullerenes considered here, the amount of

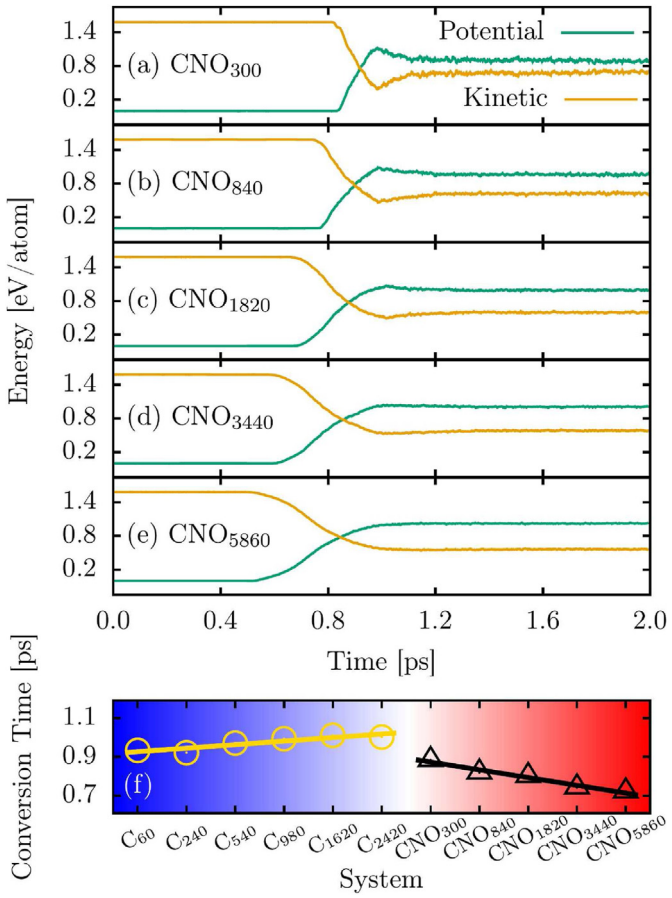

Fig. 7. Kinetic and potential energy values as a function of the simulation time during the CNO collision, for the velocity case of 5 km/s. At the bottom is also indicated compression time for the different structures. (A colour version of this figure can be viewed online.)

energy converted was approximately 0.7 eV/atom for all cases. In the conversion process, the kinetic energy dropped from 1.6 to 0.7 eV/atom, while the potential energy acquired by the CNO after the collision increased from 0 to 0.9 eV/atom. Fig. 7(f) shows that the conversion time has a linear trend for both C_N and CNO_N cases. In the C_N collision, the higher is the inner shell volume the greater is the conversion time, once the deformation degree of C_N shells increases with their volume. The CNO_N cases, in turn, presented an inverse trend. The higher is the system mass the smaller is the conversion time. The CNO_N stiffness increases with the number of shells, which makes the conversion between kinetic and potential energies faster.

4. Conclusions

In summary, we studied the dynamics and structural transformations of carbon onion-like structures under high-velocity impacts within the framework of fully atomistic reactive molecular dynamics simulations. We considered single and multi-shell nano-onions (up to six shells) and at different impact velocities (from 2 up to 7 km/s) against a fixed and rigid substrate. Our main goal was to propose a new synthesis route, based on mechanical impact of CNO against a substrate, that can be exploited in the conversion of onions to diamonds.

Our results showed the existence of three different regimes, depending on the impact velocity: slightly deformed CNO (quasi-elastic collision), collapsed CNO (inelastic collisions) forming diamondoid-like cores, and fragmented CNO yielding LACS in a gas phase of carbon atoms. CNO tend to equally distribute through their surface the amount of accumulated stress during the collision.

The impact of CNO against the substrate yielded sp^3-like bond types for all the used initial velocities. At intermediate velocities (between 3.0 and 5.0 km/s), the inelastic collision forms diamondoid-like cores by converting a substantial quantity of sp^2-like bonds into sp^3-like ones. sp^1-like bonds were also observed due to the formation of LACS. In the high velocities regime, the total number of sp^1-like, sp^2-like, and sp^3-like bonds tend to be similar, around 2000. After the CNO impact and its subsequent fragmentation, the number of sp^1-like bonds increases until the end of the simulation due to the formation of LACS.

CRediT authorship contribution statement

M.L. Pereira Júnior: Data curation, Formal analysis, Methodology, Writing – original draft. **W.F. da Cunha:** Data curation, Formal analysis, Methodology, Writing – original draft. **R.T. de Sousa Junior:** Conceptualization, Supervision, Funding acquisition, Writing – review & editing. **G.D. Amvame Nze:** Data curation, Formal analysis, Methodology, Writing – original draft. **D.S. Galvão:** Conceptualization, Supervision, Funding acquisition, Writing – review & editing. **L.A. Ribeiro Júnior:** Conceptualization, Supervision, Funding acquisition, Writing – review & editing.

Declaration of competing interest

The authors declare that they have no known competing financial interests or personal relationships that could have appeared to influence the work reported in this paper.

Acknowledgments

The authors gratefully acknowledge the financial support from Brazilian research agencies CNPq, FAPESP, and FAP-DF. M.L.P.J gratefully acknowledges the financial support from CAPES grant 88 882.383 674/2 019-01. D.S.G. thanks the Center for Computing in Engineering and Sciences at Unicamp for financial support through the FAPESP/CEPID Grants #2013/08 293-7 and #2018/11 352-7. L.A.R.J acknowledges the financial support from FAP-DF grants 00193-00000853/2021-28 and 00193-00000811/2021-97 and CNPq grant 302236/2018 – 0. L.A.R.J acknowledges CENAPAD-SP for providing the computational facilities. L.A.R.J. gratefully acknowledges the financial support from IFD/UnB (Edital 01/2020) grant 23106.090790/2020–86. The authors acknowledge the National Laboratory for Scientific Computing (LNCC/MCTI, Brazil) for providing HPC resources of the SDumont supercomputer, which have contributed to the research results reported within this paper. URL: http://sdumont.lncc.br. R.T.S.J. gratefully acknowledges CNPq (Grants 312180/2 019-5 PQ-2 and 465741/2 014-2 INCT on Cybersecurity) and DENASUS (Grant 23106.118410/2020-85).

Appendix A. Supplementary data

Supplementary data to this article can be found online at https://doi.org/10.1016/j.carbon.2021.12.064.

References

[1] L.L. Zhang, X. Zhao, Carbon-based materials as supercapacitor electrodes, Chem. Soc. Rev. 38 (2009) 2520–2531.
[2] K.P. Gopinath, D.-V.N. Vo, D.G. Prakash, A.A. Joseph, S. Viswanathan, J. Arun, Environmental applications of carbon-based materials: a review, Environ. Chem. Lett. 19 (2021) 557–582.
[3] A. Kraft, A.C. Grimsdale, A.B. Holmes, Electroluminescent conjugated

polymers—seeing polymers in a new light, Angew. Chem. Int. Ed. 37 (1998) 402–428.
[4] S. Iijima, Helical microtubules of graphitic carbon, Nature 354 (1991) 56–58.
[5] M.Y. Han, B. Özyilmaz, Y. Zhang, P. Kim, Energy band-gap engineering of graphene nanoribbons, Phys. Rev. Lett. 98 (2007), 206805.
[6] H.W. Kroto, J.R. Heath, S.C. O'Brien, R.F. Curl, R.E. Smalley, C 60: buckminsterfullerene, Nature 318 (1985) 162–163.
[7] H.-L. Zhang, J.-F. Li, B.-P. Zhang, K.-F. Yao, W.-S. Liu, H. Wang, Electrical and thermal properties of carbon nanotube bulk materials: experimental studies for the 328–958 k temperature range, Phys. Rev. B 75 (2007), 205407.
[8] G. Keru, P.G. Ndungu, V.O. Nyamori, A review on carbon nanotube/polymer composites for organic solar cells, Int. J. Energy Res. 38 (2014) 1635–1653.
[9] C. Shuttle, B. O'Regan, A. Ballantyne, J. Nelson, D.D. Bradley, J. De Mello, J. Durrant, Experimental determination of the rate law for charge carrier decay in a polythiophene: fullerene solar cell, Appl. Phys. Lett. 92 (2008) 80.
[10] X. Zhang, O.V. Yazyev, J. Feng, L. Xie, C. Tao, Y.-C. Chen, L. Jiao, Z. Pedramrazi, A. Zettl, S.G. Louie, et al., Experimentally engineering the edge termination of graphene nanoribbons, ACS Nano 7 (2013) 198–202.
[11] S. Dutta, S.K. Pati, Novel properties of graphene nanoribbons: a review, J. Mater. Chem. 20 (2010) 8207–8223.
[12] Y. Ouyang, J. Guo, A theoretical study on thermoelectric properties of graphene nanoribbons, Appl. Phys. Lett. 94 (2009), 263107.
[13] D. Abergel, V. Apalkov, J. Berashevich, K. Ziegler, T. Chakraborty, Properties of graphene: a theoretical perspective, Adv. Phys. 59 (2010) 261–482.
[14] R. Bauernschmitt, R. Ahlrichs, F.H. Hennrich, M.M. Kappes, Experiment versus time dependent density functional theory prediction of fullerene electronic absorption, J. Am. Chem. Soc. 120 (1998) 5052–5059.
[15] M.A. Greaney, S.M. Gorun, Production, spectroscopy and electronic structure of soluble fullerene ions, J. Phys. Chem. 95 (1991) 7142–7144.
[16] F. Yao, D.T. Pham, Y.H. Lee, Carbon-based materials for lithium-ion batteries, electrochemical capacitors, and their hybrid devices, ChemSusChem 8 (2015) 2284–2311.
[17] W. Lv, Z. Li, Y. Deng, Q.-H. Yang, F. Kang, Graphene-based materials for electrochemical energy storage devices: opportunities and challenges, Energy Storage Mater. 2 (2016) 107–138.
[18] P. Trogadas, T.F. Fuller, P. Strasser, Carbon as catalyst and support for electrochemical energy conversion, Carbon 75 (2014) 5–42.
[19] J. Wang, H.L. Xin, D. Wang, Recent progress on mesoporous carbon materials for advanced energy conversion and storage, Part. Part. Syst. Char. 31 (2014) 515–539.
[20] D. Ugarte, Curling and closure of graphitic networks under electron-beam irradiation, Nature 359 (1992) 707–709.
[21] M. Zeiger, N. Jäckel, V.N. Mochalin, V. Presser, Carbon onions for electrochemical energy storage, J. Mater. Chem. A 4 (2016) 3172–3196.
[22] F. Banhart, P.M. Ajayan, Carbon onions as nanoscopic pressure cells for diamond formation, Nature 382 (1996) 433–435.
[23] J. Bartelmess, S. Giordani, Carbon nano-onions (multi-layer fullerenes): chemistry and applications, Beilstein J. Nanotechnol. 5 (2014) 1980–1998.
[24] L.-C. Qin, S. Iijima, Onion-like graphitic particles produced from diamond, Chem. Phys. Lett. 262 (1996) 252–258.
[25] J. Lei, J. Liu, N. Tang, H. Han, Z. Li, K. Li, T. Zhai, H. Chen, H. Xia, Novel gram-scale synthesis of carbon nano-onions from heavy oil for supercapacitors, Adv. Mater. Interfac. 8 (2021), 2101208.
[26] M. Ghosh, S.K. Sonkar, M. Saxena, S. Sarkar, Carbon nano-onions for imaging the life cycle of drosophila melanogaster, Small 7 (2011) 3170–3177.
[27] S.K. Sonkar, M. Ghosh, M. Roy, A. Begum, S. Sarkar, Carbon nano-onions as nontoxic and high-fluorescence bioimaging agent in food chain—an in vivo study from unicellular e. coli to multicellular c. elegans, Mater. Express 2 (2012) 105–114.
[28] J. Luszczyn, M.E. Plonska-Brzezinska, A. Palkar, A.T. Dubis, A. Simionescu, D.T. Simionescu, B. Kalska-Szostko, K. Winkler, L. Echegoyen, Small noncytotoxic carbon nano-onions: first covalent functionalization with biomolecules, Chem. A Eur. J. 16 (2010) 4870–4880.
[29] M.B. Seymour, C. Su, Y. Gao, Y. Lu, Y. Li, Characterization of carbon nano-onions for heavy metal ion remediation, J. Nanoparticle Res. 14 (2012) 1–13.
[30] F.-D. Han, B. Yao, Y.-J. Bai, Preparation of carbon nano-onions and their application as anode materials for rechargeable lithium-ion batteries, J. Phys. Chem. C 115 (2011) 8923–8927.
[31] D. Su, N.I. Maksimova, G. Mestl, V.L. Kuznetsov, V. Keller, R. Schlögl, N. Keller, Oxidative dehydrogenation of ethylbenzene to styrene over ultra-dispersed diamond and onion-like carbon, Carbon 45 (2007) 2145–2151.
[32] T. Cabioc'h, E. Thune, J. Riviere, S. Camelio, J. Girard, P. Guerin, M. Jaouen, L. Henrard, P. Lambin, Structure and properties of carbon onion layers deposited onto various substrates, J. Appl. Phys. 91 (2002) 1560–1567.
[33] E. Koudoumas, O. Kokkinaki, M. Konstantaki, S. Couris, S. Korovin, P. Detkov, V. Kuznetsov, S. Pimenov, V. Pustovoi, Onion-like carbon and diamond nanoparticles for optical limiting, Chem. Phys. Lett. 357 (2002) 336–340.
[34] S. Sek, J. Breczko, M.E. Plonska-Brzezinska, A.Z. Wilczewska, L. Echegoyen, Stm-based molecular junction of carbon nano-onion, ChemPhysChem 14 (2013) 96–100.
[35] L. Hawelek, A. Brodka, S. Tomita, J. Dore, V. Honkimäki, A. Burian, Transformation of nano-diamonds to carbon nano-onions studied by x-ray diffraction and molecular dynamics, Diam. Relat. Mater. 20 (2011) 1333–1339.
[36] Y. Zheng, Y. Ma, Q. Tao, Y. Li, S. Ma, T. Cui, X. Wang, S. Dong, P. Zhu, Pressure induced structural transition of small carbon nano-onions, RSC Adv. 6 (2016) 2914–2919.
[37] M. Zaiser, F. Banhart, Radiation-induced transformation of graphite to diamond, Phys. Rev. Lett. 79 (1997) 3680.
[38] P. Wesolowski, Y. Lyutovich, F. Banhart, H. Carstanjen, H. Kronmüller, Formation of diamond in carbon onions under mev ion irradiation, Appl. Phys. Lett. 71 (1997) 1948–1950.
[39] R. Mowrey, D. Brenner, B. Dunlap, J. Mintmire, C. White, Simulations of buckminsterfullerene (c60) collisions with a hydrogen-terminated diamond {111} surface, J. Phys. Chem. 95 (1991) 7138–7142.
[40] R.D. Beck, P. St John, M.M. Alvarez, F. Diederich, R.L. Whetten, Resilience of all-carbon molecules c60, c70, and c84: a surface-scattering time-of-flight investigation, J. Phys. Chem. 95 (1991) 8402–8409.
[41] I. Ponomareva, L. Chernozatonskii, How can carbon onion transform into diamond-like structure, Microelectron. Eng. 69 (2003) 625–628.
[42] R. Clarke, C. Uher, High pressure properties of graphite and its intercalation compounds, Adv. Phys. 33 (1984) 469–566.
[43] J.C. Angus, C.C. Hayman, Low-pressure, metastable growth of diamond and "diamond like" phases, Science 241 (1988) 913–921.
[44] E.F. Oliveira, P.A. da Silva Autreto, D.S. Galvão, On hardening silver nanocubes by high-velocity impacts: a fully atomistic molecular dynamics investigation, J. Mater. Sci. 53 (2018) 7486–7492.
[45] S. Ozden, P.A. Autreto, C.S. Tiwary, S. Khatiwada, L. Machado, D.S. Galvao, R. Vajtai, E.V. Barrera, P.M. Ajayan, Unzipping carbon nanotubes at high impact, Nano Lett. 14 (2014) 4131–4137.
[46] E. Armani, P.A. Autreto, High-velocity impact of a hybrid cbn nanotubes, Oxford Open Mater. Sci. 1 (2021), itaa006.
[47] C.F. Woellner, L.D. Machado, P.A. Autreto, J.M. de Sousa, D.S. Galvao, Structural transformations of carbon and boron nitride nanoscrolls at high impact collisions, Phys. Chem. Chem. Phys. 20 (2018) 4911–4916.
[48] J.M. de Sousa, L.D. Machado, C.F. Woellner, P.A. da Silva Autreto, D.S. Galvao, Carbon nanoscrolls at high impacts: a molecular dynamics investigation, MRS Adv. 1 (2016) 1423–1428.
[49] H. Qi, S. Picaud, M. Devel, E. Liang, Z. Wang, Adsorption of organic molecules on onion-like carbons: insights on the formation of interstellar hydrocarbons, Astrophys. J. 867 (2018) 133.
[50] A.C. Van Duin, S. Dasgupta, F. Lorant, W.A. Goddard, Reaxff: a reactive force field for hydrocarbons, J. Phys. Chem. A 105 (2001) 9396–9409.
[51] C. Ashraf, A.C. Van Duin, Extension of the reaxff combustion force field toward syngas combustion and initial oxidation kinetics, J. Phys. Chem. A 121 (2017) 1051–1068.
[52] S. Plimpton, Fast parallel algorithms for short-range molecular dynamics, J. Comput. Phys. 117 (1995) 1–19, https://doi.org/10.1006/jcph.1995.1039.
[53] W. Humphrey, A. Dalke, K. Schulten, et al., Vmd: visual molecular dynamics, J. Mol. Graph. 14 (1996) 33–38.
[54] W.G. Hoover, Canonical dynamics: equilibrium phase-space distributions, Phys. Rev. A 31 (1985) 1695.
[55] L.C. Felix, R.M. Tromer, P.A. Autreto, L.A. Ribeiro Junior, D.S. Galvao, On the mechanical properties and thermal stability of a recently synthesized monolayer amorphous carbon, J. Phys. Chem. C 124 (2020) 14855–14860.